

# Bounds on the electromagnetic dipole moments through the single top production at the CLIC

M. Köksal<sup>\*,1</sup> A. A. Billur<sup>†,2</sup> and A. Gutiérrez-Rodríguez<sup>‡3</sup>

<sup>1</sup>*Department of Optical Engineering, Cumhuriyet University, 58140, Sivas, Turkey.*

<sup>2</sup>*Department of Physics, Cumhuriyet University, 58140, Sivas, Turkey.*

<sup>3</sup>*Facultad de Física, Universidad Autónoma de Zacatecas*

*Apartado Postal C-580, 98060 Zacatecas, México.*

(Dated: December 3, 2024)

## Abstract

We obtain bounds on the anomalous magnetic and electric dipole moments of the  $t$ -quark from a future high-energy and high-luminosity linear electron positron collider, such as the CLIC, with unpolarized and polarized electron beams which are a powerful tool to determine new physics. We consider the processes  $\gamma e^- \rightarrow \bar{t} b \nu_e$  ( $\gamma$  is the Compton backscattering photon) and  $e^+ e^- \rightarrow e^- \gamma^* e^+ \rightarrow \bar{t} b \nu_e e^+$  ( $\gamma^*$  is the Weizsacker-Williams photon) which are one of the most important sources of single top quark production. For the systematic uncertainties of  $\delta_{sys} = 0\%$ ,  $5\%$ ,  $b$  – tagging efficiency = 0.8, center-of-mass energy of  $\sqrt{s} = 3 \text{ TeV}$ , integrated luminosity of  $\mathcal{L} = 2 \text{ ab}^{-1}$  and  $2\sigma$  ( $3\sigma$ ) C.L. the future  $e^+ e^-$  collider may put bounds on the electromagnetic dipole moments  $\hat{a}_V$  and  $\hat{a}_A$  of the top quark of the order of  $\mathcal{O}(10^{-2} - 10^{-1})$ , which are highly competitive with those recently reported in previous studies.

PACS numbers: 14.65.Ha, 13.40.Em

Keywords: Top quarks, Electric and Magnetic Moments.

---

\* mkoksal@cumhuriyet.edu.tr

† abillur@cumhuriyet.edu.tr

‡ alexgu@fisica.uaz.edu.mx

## I. INTRODUCTION

The top quark is by far the heaviest particle of the Standard Model (SM) [1–3], its mass is  $m_t = 173.5 \pm 0.6$  (stat.)  $\pm 0.8$  (syst.) [4]. Up to now, the top quark has only been studied at hadron colliders, at the Tevatron and at the Large Hadron Collider (LHC). Its large mass implies that the top quark is the SM particle most strongly coupled to the mechanism of electroweak symmetry breaking. Mainly for this and other reasons, it is considered to be one of the most likely places where new physics might be discovered, which is to say, the top quark is a window to any new physics at the  $TeV$  energy scale. While enough information about the top quark is already available, showing consistency with SM expectations, its properties and interactions are among the most important measurements for present and future high energy colliders [5–13].

The construction of a high-energy  $e^+e^-$  International Linear Collider (ILC) has been proposed to complement direct searches carried at the LHC. In the case of the top quark, precision measurements of its properties, in particular of its couplings, are specially interesting because it is the heaviest elementary particle yet discovered, and thus, it is expected to be more sensitive to new physics at higher scales.

While the top quark has been studied in some detail at the Tevatron and LHC, many of its properties besides the mass, spin, the color and electric charges, the electric and magnetic dipole moments and the chromomagnetic and chromoelectric dipole moments are still poorly constrained. Significant new insights on top quark properties will therefore be one of the tasks of the LHC, the ILC [7–9] and the Compact Linear Collider (CLIC) [11, 14].

Some the most sensitive observable of the top quark are their dipole moments, and although these intrinsic properties have been studied extensively, both theoretically and experimentally, it is necessary to have more precise measurements on the dipole moments of the top quark. The dipole moments of the top quark has been investigated by several authors and in a variety of theoretical models [15–22]. Further, a number of analysis shows that in the processes  $e^+e^- \rightarrow t\bar{t}$  and  $\gamma\gamma \rightarrow t\bar{t}$  the dipole moments of the top quark can be measured with great sensitivity [23–26]. However, there are a significant number of top quarks that are produced singly, via the weak interaction. There are several single top quark production processes of interest in  $e^+e^-$ ,  $e^-e^-$ ,  $\gamma e^-$  and  $\gamma\gamma$  collisions, which may be characterised by the virtuality of the W boson [27–36].

Although it has not been given the importance it deserves the study on the single top quarks production, there are several reasons why our study is necessary in future linear  $e^+e^-$  colliders: 1) It is a very good alternative to study the dipole moments  $\hat{a}_V$  and  $\hat{a}_A$  of the top quark, as well as the anomalous coupling  $tbW$ . 2) Single top production at CLIC in association with a  $W$  boson and bottom quark through  $WW^*$  production leads to the same final state as  $t$  quark pair production. 3) The cross section for single top quark production processes is significant since the single top quark production is abundant in  $e^+e^-$  colliders that operate at high energies. In addition, the single top quark production is directly proportional to the square of the  $tbW$  coupling, and therefore it is potentially very sensitive to the  $tbW$  structure [37]. 4) Single top quarks are produced with nearly 100% polarization, due to the weak interaction [38, 39]. 5) New physics may be discernible in single top quark production processes. New physics can influence single top production by inducing beyond the SM weak interactions [39, 40], through loop effects [41–43], or by providing new sources of single top quark production [44–46]. These are some of the reasons why it is attractive to study the properties of the top quark, especially their dipole moments through the single top quark production processes.

In the SM the prediction for the Magnetic Dipole Moment (MDM) of the top quark is  $a_t^{SM} = 0.02$  [47], which can be tested in the current and future colliders, which is to say, LHC and CLIC. In contrast, the Electric Dipole Moment (EDM) of the top quark is strongly suppressed and is less than  $10^{-30}$  ecm [15, 48, 49], much too small to be observed. However, is highly attractive for probing new physics.

The sensitivity to the EDM has been studied in models with vector like multiplets, which predicted the top quark EDM close to  $1.75 \times 10^{-3}$  [50].

There are studies performed via the  $t\bar{t}\gamma$  production for the LHC at  $\sqrt{s} = 14 \text{ TeV}$  and  $\mathcal{L} = 300 \text{ fb}^{-1}$  and  $3000 \text{ fb}^{-1}$ , reporting the limits of  $\pm 0.2$  and  $\pm 0.1$ , respectively [51]. Other limits are reported in the literature:  $-2.0 \leq \hat{a}_V \leq 0.3$  and  $-0.5 \leq \hat{a}_A \leq 1.5$  which are obtained from the branching ratio and the CP asymmetry from radiative  $b \rightarrow s\gamma$  transitions [52], while the bounds of  $|\hat{a}_V| < 0.05$  (0.09) and  $|\hat{a}_A| < 0.20$  (0.28) comes from measurements of  $\gamma p \rightarrow t\bar{t}$  cross section with 10% (18%) uncertainty, respectively [53]. More recent limits on the top quark magnetic and electric dipole moments through the process  $pp \rightarrow p\gamma^*\gamma^*p \rightarrow pt\bar{t}p$  at the LHC with  $\sqrt{s} = 14 \text{ TeV}$ ,  $\mathcal{L} = 3000 \text{ fb}^{-1}$  and 68% C.L. are  $-0.6389 \leq \hat{a}_V \leq 0.0233$  and  $|\hat{a}_A| \leq 0.1158$  [54]. Sensitivity limits for the anomalies couplings of the top quark through

the process of production of top quark pairs  $e^+e^- \rightarrow t\bar{t}$  for the ILC at  $\sqrt{s} = 500 \text{ GeV}$ ,  $\mathcal{L} = 200 \text{ fb}^{-1}$ ,  $\mathcal{L} = 300 \text{ fb}^{-1}$  and  $\mathcal{L} = 500 \text{ fb}^{-1}$  are predicted to be of the order of  $\mathcal{O}(10^{-3})$ , which is to say, the measurements at an electron positron collider lead to a significant improvement in comparison with LHC. Detailed discussions on the dipole moments of the top quark in top quark pairs production at the ILC are reported in the literature [7–10, 13, 23–26, 55–57]. It is worth mentioning that do not limits exist reported in the literature on the dipole moments  $\hat{a}_V$  and  $\hat{a}_A$  via single top quark production processes.

CP violation was firstly observed in a small fractions of  $K$  mesons decaying to two pions in the SM. This phenomenology in the SM can be easily introduced by the Cabibbo-Kobayashi-Maskawa mechanism in the quark sector. But, CP violation in this mechanism is not enough to explain the matter-antimatter asymmetry in the universe. For this reason, the presence of new physics beyond the SM can be investigated by examining the electromagnetic properties of the top quark that are defined with CP-symmetric and CP-asymmetric anomalous form factors. Its dipole moments such as the MDM coming from one-loop level perturbations and the corresponding EDM, which is described as a source of CP violation.

Following references [51, 54, 58–60], the definition of the general effective coupling  $t\bar{t}\gamma$  including the SM coupling and contributions from dimension-six effective operators can be parameterized by the following effective Lagrangian:

$$\mathcal{L}_{\gamma t\bar{t}} = -g_e Q_t \bar{t} \Gamma_{\gamma t\bar{t}}^\mu t A_\mu, \quad (1)$$

where  $g_e$  is the electromagnetic coupling constant,  $Q_t$  is the top quark electric charge and the Lorentz-invariant vertex function  $\Gamma_{\gamma t\bar{t}}^\mu$  which describes the interaction of a  $\gamma$  photon with two top quarks can be parameterized by

$$\Gamma_{\gamma t\bar{t}}^\mu = \gamma^\mu + \frac{i}{2m_t} (\hat{a}_V + i\hat{a}_A \gamma_5) \sigma^{\mu\nu} q_\nu, \quad (2)$$

where  $m_t$  is the mass of the top quark,  $q$  is the momentum transfer to the photon and the couplings  $\hat{a}_V$  and  $\hat{a}_A$  are real and related to the anomalous magnetic moment and the electric dipole moment of the top quark, respectively.

The linear colliders may have another option that polarized beam collisions. These type of collisions give new perspectives such as on the hadronic structure and high precision measurements on the electroweak mixing angle. Beam polarization could be important role

in the next linear colliders as well as RHIC and HERA. It is expected that about 80% polarization of lepton beam can be achivable at the future linear colliders. In this work, we take into account one beam can be  $-80\%$  polarization. It is worth mentioning that the polarization  $P_{e-} = -80\%$  enhances the cross sections according to the unpolarized case.

In this work we study the sensibility of the anomalous magnetic and electric dipole moments of the top quark through the processes  $\gamma e^- \rightarrow \bar{t} b \nu_e$  ( $\gamma$  is the Compton backscattering photon) and  $e^+ e^- \rightarrow e^- \gamma^* e^+ \rightarrow \bar{t} b \nu_e e^+$  ( $\gamma^*$  is the Weizsacker-Williams photon) which are one of the most important sources of single top quark production [27, 30]. We use center-of-mass energies of the CLIC in this work [14]. These values are for a center-of-mass energy of  $1.4 \text{ TeV}$  with integrated luminosity of  $1500 \text{ fb}^{-1}$  and  $3 \text{ TeV}$  with  $\mathcal{L} = 2000 \text{ fb}^{-1}$ , with unpolarized and polarized electron beams, which is to say,  $P_{e-} = -80\%$  and  $P_{e+} = 0\%$  [61]. Not only can the future  $e^+ e^-$  linear collider be designed to operate in  $e^+ e^-$  collision mode, but it can also be operated as a  $e\gamma$  and  $\gamma\gamma$  collider. This is achieved by using Compton backscattered photons in the scattering of intense laser photons on the initial  $e^+ e^-$  beams. The other well-known applications of linear colliders are to study new physics beyond the SM through  $e\gamma^*$  and  $\gamma^*\gamma^*$  collisions. A quasisreal  $\gamma^*$  photon emitted from one of the incoming  $e^-$  or  $e^+$  beams can interact with the other lepton shortly after, and the subprocess  $\gamma^* e^- \rightarrow \bar{t} b \nu_e$  can generate. Hence, first, we calculate the main reaction  $e^+ e^- \rightarrow e^- \gamma^* e^+ \rightarrow \bar{t} b \nu_e e^+$  by integrating the cross section for the subprocess  $\gamma^* e^- \rightarrow \bar{t} b \nu_e$ . In this case, the quasisreal photons in  $\gamma^* e^-$  collisions can be examined by Equivalent Photon Approximation (EPA) [62–64], which is to say, by using the Weizsacker-Williams approximation (WWA). Also, we can add part related to the large values of  $Q_{max}^2$  which do not bring an important contribution to obtain sensitivity limits on the anomalous couplings [65–68]. In EPA, photons emitted from incoming leptons which have very low virtuality are scattered at very small angles from the beam pipe and because the emitted quasisreal photons have a low  $Q^2$  virtuality these are almost real. We use only the photon virtuality of  $Q_{max}^2 = 2 \text{ GeV}^2$ . These processes have been observed phenomenologically and experimentally at the LEP, Tevatron and LHC [69–90].

With these motivations, we study the potential of the processes  $\gamma e^- \rightarrow \bar{t} b \nu_e$  and  $e^+ e^- \rightarrow e^+ \gamma^* e^- \rightarrow \bar{t} b \nu_e e^+$  via Compton backscattering and WWA, respectively and derive bounds on the dipole moments  $\hat{a}_V$  and  $\hat{a}_A$  at  $2\sigma$  and  $3\sigma$  level (90% and 95% C.L.), and at a future high-energy and high-luminosity linear electron positron collider, such as the CLIC to study the sensibility on the anomalous magnetic and electric dipole moments of the top quark.

For this we calculate the main reaction  $e^+e^- \rightarrow e^-\gamma^*e^+ \rightarrow \bar{t}b\nu_e e^+$  by integrating the cross section for the subprocess  $\gamma^*e^- \rightarrow \bar{t}b\nu_e$ . In this case, while lepton emitted photon is not detect by the central detector, the other particles are detect in the central detectors. We also present the results for the  $b$ -tagging efficiency of 0.8, systematic uncertainty of  $\delta_{sys} = 5\%$  and the acceptance cuts will imposed as  $|\eta^b| < 2.5$  for pseudorapidity,  $p_T^b > 20 \text{ GeV}$  and  $p_T^{\nu_e} > 10 \text{ GeV}$  for transverse momentums of the final state particles. In addition, for this we consider hadronic decay channels of the top quark, which is to say,  $BR = 0.676$  (Hadronic branching ratio). The corresponding schematic and Feynman diagrams for the main reactions as well as for the subprocesses which give the most important contribution to the total cross section are shown in Figs. 1-2.

To illustrate our results for both processes we show the dependence of the total cross section as a function of the magnetic moment and electric dipole moments  $\hat{a}_V$  and  $\hat{a}_A$  of the top quark for two different values of the center-of-mass energies 1.4 and 3  $TeV$ , respectively. We also include a contours plot for the upper bounds of the anomalous couplings  $\hat{a}_V$  and  $\hat{a}_A$  with 95% C.L. for different values of the center-of-mass energies  $\sqrt{s} = 1.4, 3 \text{ TeV}$  with corresponding maximum luminosities for both processes. The sensitivity limits on the magnetic moment  $\hat{a}_V$  and the electric dipole moment  $\hat{a}_A$  of the top quark for some values of the center-of-mass energy and luminosity are also calculated.

This paper is organized as follows. In Section II, we study the dipole moments of the top quark through the process  $\gamma e^- \rightarrow \bar{t}b\nu_e$ . In Section III, we study the dipole moments of the top quark through the process  $e^+e^- \rightarrow e^+\gamma^*e^- \rightarrow \bar{t}b\nu_e e^+$ . Finally, we present our results and conclusions in Section IV.

## II. COMPTON BACKSCATTERING: CROSS SECTION OF $\gamma e^- \rightarrow \bar{t}b\nu_e$

In order to realized our study, in this section we present numerical results of the cross section for the process  $\gamma e^- \rightarrow \bar{t}b\nu_e$ , for this we use the CalcHEP [91, 92] packages for calculations of the matrix elements and cross sections. These packages provide automatic computation of the cross sections and distributions in the SM as well as their extensions at tree level. We consider the high-energy stage of possible future linear  $\gamma e^-$  collisions with  $\sqrt{s} = 1.4$  and 3  $TeV$  and design luminosity 50, 300, 500, 1000, 1500 and 2000  $fb^{-1}$  according to the new data reported by the CLIC [14]. In addition, we consider the acceptance cuts

of  $|\eta^b| < 2.5$  for pseudorapidity,  $p_T^b > 20 \text{ GeV}$  and  $p_T^{\nu_e} > 10 \text{ GeV}$  for transverse momentum of the final state particles. We also consider the hadronic decay channels of the top quark, which is to say,  $BR = 0.676$  and  $b$ -tagging efficiency of 0.8. Furthermore, we add the systematic error to our cross section calculations. For hadron colliders there are systematic uncertainties for single top quark production [93]. For example these uncertainties arise from luminosity, jet identification, backgrounds,  $b$  – tagging efficiency, etc.. On the other hand, linear colliders have less uncertainties with respect to hadron colliders for determination of cross section of single top quark production [94]. Therefore, for events estimation in  $\chi^2$  analysis, we have taken in account  $b$  – tagging efficiency as well as we consider systematic uncertainties of 0% and 5%. The values close to this systematic uncertainty value have been taken into account in previous studies for example Ref. [95] has been assumed a 3% systematic error in the total cross section for the  $e^-e^+ \rightarrow t\bar{t}$  process at the ILC. Also, it can see that the systematic error in the cross section determination has been lowered from 3% to 1% [96]. However, since there is no any study related to the systematic error on the single top quark production at the CLIC, we take systematic errors of 0% and 5% for the processes studied in this paper.

In our study, we examined the projected  $2\sigma$  and  $3\sigma$  sensitivities on the dipole moments  $\hat{a}_V$  and  $\hat{a}_A$  of the top quark for the processes  $\gamma e^- \rightarrow \bar{t}b\nu_e$  ( $\gamma$  is the Compton backscattering photon) and  $e^+e^- \rightarrow e^-\gamma^*e^+ \rightarrow \bar{t}b\nu_e e^+$  ( $\gamma^*$  is the Weizsacker-Williams photon) at the CLIC-1.4  $TeV$  and CLIC-3  $TeV$ , respectively, for this, we use chi-squared test. The chi-squared distribution test is defined as

$$\chi^2 = \left( \frac{\sigma_{SM} - \sigma_{NP}(\hat{a}_V, \hat{a}_A)}{\sigma_{SM}\delta} \right)^2, \quad (3)$$

where  $\sigma_{NP}(\hat{a}_V, \hat{a}_A)$  is the total cross section including contributions from the SM and New physics,  $\delta = \sqrt{(\delta_{st})^2 + (\delta_{sys})^2}$ ,  $\delta_{st} = \frac{1}{\sqrt{N_{SM}}}$  is the statistical error,  $\delta_{sys}$  is the systematic error and  $N_{SM}$  is the number of signal expected events  $N_{SM} = \mathcal{L}_{int} \times BR \times \sigma_{SM} \times \epsilon_b$  where  $\epsilon_b = 0.8$  is the  $b$  – tagging efficiency and  $\mathcal{L}_{int}$  is the integrated CLIC luminosity.

### A. Top quark dipole moments through the process $\gamma e^- \rightarrow \bar{t} b \nu_e$ with polarized beams

With polarized beams of electrons and positrons, the cross section of a process can be expressed as [61]

$$\begin{aligned} \sigma(P_{e^-}, P_{e^+}) = & \frac{1}{4}[(1 + P_{e^-})(1 + P_{e^+})\sigma_{++} + (1 - P_{e^-})(1 - P_{e^+})\sigma_{--} \\ & + (1 + P_{e^-})(1 - P_{e^+})\sigma_{+-} + (1 - P_{e^-})(1 + P_{e^+})\sigma_{-+}], \end{aligned} \quad (4)$$

where  $P_{e^-}$  ( $P_{e^+}$ ) is the polarization degree of the electron (positron) beam, while  $\sigma_{-+}$  stands for the cross section for completely left-handed polarized  $e^-$  beam  $P_{e^-} = -1$  and completely right-handed polarized  $e^+$  beam  $P_{e^+} = 1$ , and other cross sections  $\sigma_{--}$ ,  $\sigma_{++}$  and  $\sigma_{+-}$  are defined analogously. For the numerical analysis of the process  $\gamma e^- \rightarrow \bar{t} b \nu_e$ , we consider unpolarized and polarized electron beams, which is to say,  $P_{e^-} = -80\%$  and  $P_{e^+} = 0\%$ .

The corresponding Feynman diagrams for the process  $\gamma e^- \rightarrow \bar{t} b \nu_e$  that give the most important contribution to the total cross sections are shown in Fig. 2. From Fig. 2, the Feynman diagrams (1)-(3) correspond to the contribution of the SM, while diagram (4) corresponds to the anomalous contribution, which is to say, for the  $\gamma e^-$  collisions there are SM background at the tree level so the total cross section is proportional to  $\sigma_{Tot} = \sigma_{SM} + \sigma_{Int}(\hat{a}_V, \hat{a}_A) + \sigma_{Anom}(\hat{a}_V^2, \hat{a}_A^2, \hat{a}_V \hat{a}_A)$ , respectively.

To illustrate our results we show the dependence of the cross section on the anomalous couplings  $\hat{a}_V$  and  $\hat{a}_A$  for  $\gamma e^- \rightarrow \bar{t} b \nu_e$  in Fig. 3 for  $P_{e^-} = -80\%$ ,  $P_{e^+} = 0\%$  [61] and two different center-of-mass energies  $\sqrt{s} = 1.4, 3 \text{ TeV}$  [14], whereas the  $\hat{a}_V$  ( $\hat{a}_A$ ) anomalous coupling is kept fixed at zero. We observed that the cross section is sensitive to the value of the center-of-mass energies. The sensitivity to  $\bar{t} b \nu_e$  increases with the collider energy reaching a maximum at the end of the range considered:  $\hat{a}_{V,A} = \pm 1$ . At the end of this range, the cross section for  $\sqrt{s} = 3 \text{ TeV}$  increases relative to  $\sqrt{s} = 1.4 \text{ TeV}$  up to 24.5%. By contrast, in the vicinity of  $\hat{a}_{V,A} = 0$  the total cross section is smaller. We notice that, as shown in Fig. 3, the  $\gamma e^- \rightarrow \bar{t} b \nu_e$  production process at an CLIC-based  $\gamma e^-$  collider reaches a value of  $\sigma = 0.55 \text{ pb}$  for  $\sqrt{s} = 3 \text{ TeV}$ . The obvious conclusion is that in this case the  $t\bar{t}\gamma$  coupling could be probed with remarkable sensitivity (see Table I).

In Fig. 4 we used two center-of-mass energies  $\sqrt{s} = 1.4, 3 \text{ TeV}$  planned for the CLIC



TABLE I: Bounds on the  $\hat{a}_V$  magnetic moment and  $\hat{a}_A$  electric dipole moment for the process  $\gamma e^- \rightarrow \bar{t}b\nu_e$  ( $\gamma$  is the Compton backscattering photon) for  $P_{e^-,e^+} = -80\%, 0\%$ ,  $b$ -tagging efficiency = 0.8,  $\delta_{sys} = 0\%, 5\%$  at  $2\sigma$  and  $3\sigma$  C.L.

2 $\sigma$ C.L.		$\delta_{sys} = 0\%$		$\delta_{sys} = 5\%$	
$\sqrt{s}$ (TeV)	$\mathcal{L}$ ( $fb^{-1}$ )	$\hat{a}_V$	$ \hat{a}_A $	$\hat{a}_V$	$ \hat{a}_A $
1.4	50	[-0.1091, 0.1565]	0.1615	[-0.1902, 0.2406]	0.2352
1.4	300	[-0.0630, 0.1103]	0.1032	[-0.1785, 0.2289]	0.2235
1.4	500	[-0.0534, 0.1007]	0.0908	[-0.1775, 0.2279]	0.2224
1.4	1000	[-0.0424, 0.0897]	0.0763	[-0.1767, 0.2271]	0.2217
1.4	1500	[-0.0369, 0.0842]	0.0689	[-0.1765, 0.2268]	0.2214
3	50	[-0.0724, 0.0816]	0.0768	[-0.1163, 0.1254]	0.1208
3	300	[-0.0447, 0.0539]	0.0491	[-0.1120, 0.1211]	0.1164
3	500	[-0.0389, 0.0480]	0.0432	[-0.1116, 0.1207]	0.1161
3	1000	[-0.0320, 0.0412]	0.0364	[-0.1113, 0.1204]	0.1158
3	1500	[-0.0286, 0.0377]	0.0329	[-0.1113, 0.1203]	0.1157
3	2000	[-0.0234, 0.0325]	0.0277	[-0.1112, 0.1203]	0.1156
3 $\sigma$ C.L.		$\delta_{sys} = 0\%$		$\delta_{sys} = 5\%$	
1.4	50	[-0.1209, 0.1683]	0.1762	[-0.2096, 0.2599]	0.2567
1.4	300	[-0.0703, 0.1177]	0.1126	[-0.1968, 0.2472]	0.2438
1.4	500	[-0.0598, 0.1071]	0.0990	[-0.1957, 0.2460]	0.2427
1.4	1000	[-0.0477, 0.0950]	0.0833	[-0.1948, 0.2452]	0.2418
1.4	1500	[-0.0416, 0.0889]	0.0752	[-0.1945, 0.2449]	0.2416
3	50	[-0.0794, 0.0886]	0.0838	[-0.1273, 0.1364]	0.1318
3	300	[-0.0492, 0.0583]	0.0535	[-0.1226, 0.1317]	0.1270
3	500	[-0.0428, 0.0520]	0.0472	[-0.1222, 0.1313]	0.1266
3	1000	[-0.0353, 0.0445]	0.0396	[-0.1219, 0.1310]	0.1263
3	1500	[-0.0315, 0.0407]	0.0358	[-0.1218, 0.1309]	0.1262
3	2000	[-0.0258, 0.0350]	0.0301	[-0.1217, 0.1308]	0.1261

accelerator in order to get contours limits in the plane  $\hat{a}_V - \hat{a}_A$  for  $\gamma e^- \rightarrow \bar{t}b\nu_e$  and the planned luminosities of  $\mathcal{L} = 50, 500, 1500, 2000 \text{ fb}^{-1}$  and  $b$ -tagging efficiency = 0.8.

As an indicator of the order of magnitude, in Table I with  $b$ -tagging efficiency of 0.8 and considering the systematic errors of  $\delta_{sys} = 0\%, 5\%$  we present the bounds obtained on the  $\hat{a}_V$  magnetic moment and  $\hat{a}_A$  electric dipole moments of the  $t$ -quark with the polarization  $P_{e-} = -80\%$  for the electron beams and  $P_{e+} = 0\%$  for the positron and  $\sqrt{s} = 1.4, 3 \text{ TeV}$ ,  $\mathcal{L} = 50, 300, 500, 1000, 1500, 2000 \text{ fb}^{-1}$  at  $2\sigma$  and  $3\sigma \text{ C.L.}$ , respectively. As expected, our results presented in Table I clearly show that as the energy and luminosity of the collider increases, the bounds on the dipole moments of the top quark are stronger. We observed that the results obtained in Table I are competitive with those recently reported in previous studies [51–54]. From results presented in Table I, it is obvious that the effect of polarized beams is more significant than in the case of unpolarized beams (see Table II).

## B. Top quark dipole moments through the process $\gamma e^- \rightarrow \bar{t}b\nu_e$ with unpolarized beams

Following a similar procedure as in subsection A, we show our results for the total cross section on the anomalous couplings  $\hat{a}_V$  and  $\hat{a}_A$  for the process  $\gamma e^- \rightarrow \bar{t}b\nu_e$  with unpolarized beams, which is one of the most important sources of single top quark production. In Fig. 5, our results are presented for two different center-of-mass energies  $\sqrt{s} = 1.4, 3 \text{ TeV}$ . The cross section for  $\gamma e^- \rightarrow \bar{t}b\nu_e$  is sensitive to the value of the center-of-mass energies and this sensitivity to  $\bar{t}b\nu_e$  increases with the collider energy reaching a maximum at the end of the range considered, which is to say,  $\hat{a}_{V,A} = \pm 1$ . Comparing the curves in Fig. 5, we see that the sensitivity of the cross section for the center-of-mass energies of  $\sqrt{s} = 1.4$  and  $3 \text{ TeV}$  increases up to 26.6% at the ends of the interval considered. The opposite effect is observed in the vicinity of  $\hat{a}_{V,A} = 0$  where the cross section is smaller. We notice that, as shown in Fig. 5, the  $\gamma e^- \rightarrow \bar{t}b\nu_e$  production process at an CLIC-based  $\gamma e^-$  collider reaches a value of  $\sigma = 0.3 \text{ pb}$  for  $\sqrt{s} = 3 \text{ TeV}$ . The evident conclusion is that in this case the cross section is approximately the half of the polarized case, however even in these conditions the  $\gamma t\bar{t}$  coupling could be probed with remarkable sensitivity (see Table II).

In Fig. 6 we used two center-of-mass energies  $\sqrt{s} = 1.4, 3 \text{ TeV}$  planned for the CLIC accelerator in order to get contours limits in the plane  $\hat{a}_V - \hat{a}_A$  for  $\gamma e^- \rightarrow \bar{t}b\nu_e$  with the

TABLE II: Bounds on the  $\hat{a}_V$  magnetic moment and  $\hat{a}_A$  electric dipole moment for the process  $\gamma e^- \rightarrow \bar{t} b \nu_e$  ( $\gamma$  is the Compton backscattering photon) for  $b$  – tagging efficiency = 0.8,  $\delta_{sys} = 0\%$ , 5% at  $2\sigma$  and  $3\sigma$  C.L.

2 $\sigma$ C.L.		$\delta_{sys} = 0\%$		$\delta_{sys} = 5\%$	
$\sqrt{s}$ (TeV)	$\mathcal{L}$ ( $fb^{-1}$ )	$\hat{a}_V$	$ \hat{a}_A $	$\hat{a}_V$	$ \hat{a}_A $
1.4	50	[-0.1624, 0.2158]	0.1872	[-0.2198, 0.2733]	0.2451
1.4	300	[-0.0958, 0.1493]	0.1196	[-0.2003, 0.2538]	0.2255
1.4	500	[-0.0882, 0.1353]	0.1052	[-0.1985, 0.2520]	0.2237
1.4	1000	[-0.0657, 0.1192]	0.0885	[-0.1971, 0.2506]	0.2223
1.4	1500	[-0.0576, 0.1111]	0.0800	[-0.1967, 0.2501]	0.2218
3	50	[-0.0845, 0.0936]	0.0887	[-0.1201, 0.1292]	0.1246
3	300	[-0.0523, 0.0614]	0.0563	[-0.1127, 0.1218]	0.1172
3	500	[-0.0454, 0.0545]	0.0494	[-0.1120, 0.1212]	0.1165
3	1000	[-0.0375, 0.0465]	0.0414	[-0.1115, 0.1207]	0.1160
3	1500	[-0.0334, 0.0425]	0.0373	[-0.1114, 0.1205]	0.1159
3	2000	[-0.0273, 0.0364]	0.0312	[-0.1113, 0.1204]	0.1158
3 $\sigma$ C.L.		$\delta_{sys} = 0\%$		$\delta_{sys} = 5\%$	
1.4	50	[-0.1793, 0.2327]	0.2043	[-0.2420, 0.2955]	0.2674
1.4	300	[-0.1065, 0.1599]	0.1305	[-0.2207, 0.2742]	0.2460
1.4	500	[-0.0912, 0.1447]	0.1149	[-0.2188, 0.2722]	0.2440
1.4	1000	[-0.0735, 0.1269]	0.0969	[-0.2172, 0.2707]	0.2425
1.4	1500	[-0.0645, 0.1180]	0.0873	[-0.2167, 0.2702]	0.2420
3	50	[-0.0926, 0.1017]	0.0966	[-0.1315, 0.1406]	0.1360
3	300	[-0.0574, 0.0665]	0.0616	[-0.1234, 0.1325]	0.1279
3	500	[-0.0500, 0.0591]	0.0541	[-0.1226, 0.1318]	0.1271
3	1000	[-0.0413, 0.0504]	0.0453	[-0.1221, 0.1312]	0.1266
3	1500	[-0.0368, 0.0459]	0.0408	[-0.1219, 0.1310]	0.1264
3	2000	[-0.0301, 0.0392]	0.0341	[-0.1218, 0.1309]	0.1263

planned luminosities of  $\mathcal{L} = 50, 500, 1500, 2000 \text{ fb}^{-1}$  and  $b$ -tagging efficiency = 0.8.

In Table II we present the bounds obtained on the  $\hat{a}_V$  magnetic moment and  $\hat{a}_A$  electric dipole moments of the top quark for  $\sqrt{s} = 1.4, 3 \text{ TeV}$  and  $\mathcal{L} = 50, 300, 500, 1000, 1500, 2000 \text{ fb}^{-1}$  at  $2\sigma$  and  $3\sigma \text{ C.L.}$ , respectively. The final value adopted for the center-of-mass energy of  $\sqrt{s} = 3 \text{ TeV}$  and the integrated luminosity of  $\mathcal{L} = 2 \text{ ab}^{-1}$  at  $2\sigma$  and  $3\sigma$ , is the most sensitive interval to the  $\hat{a}_V$  ( $\hat{a}_A$ ). Increasing the  $\sqrt{s}$  as well as the  $\mathcal{L}$  provide more restricted bounds on both the anomalous couplings  $\hat{a}_V$  and  $\hat{a}_A$ . We observed that the results obtained in Table II are competitive with those recently reported in previous studies [51–54].

Comparison of Tables I and II clearly shows that the effects of the polarized electron beams  $P_{e^-,e^+} = -80\%, 0\%$  enhances the total cross section as well as improving the bounds on the dipole moments of the top quark, according to the unpolarized beams case. In addition, that we assume a efficiency of 0.8 for tagging the b-quark and considering the systematic errors of 0% and 5%, respectively.

### III. WEIZSACKER-WILLIAMS APPROXIMATION: CROSS SECTION OF

$$e^+e^- \rightarrow e^+\gamma^*e^- \rightarrow \bar{t}b\nu_e e^+$$

In this section we study the dipole moments of the top quark via the process  $e^+e^- \rightarrow e^+\gamma^*e^- \rightarrow \bar{t}b\nu_e e^+$ , with unpolarized and polarized  $e^-$  beams and for the center-of-mass energies of the CLIC [14].

#### A. Top quark dipole moments through the process $e^+e^- \rightarrow e^+\gamma^*e^- \rightarrow \bar{t}b\nu_e e^+$ with polarized beams

The corresponding Feynman diagrams for the subprocess  $\gamma^*e^- \rightarrow \bar{t}b\nu_e$  that give the most important contribution to the total cross section are shown in Fig. 2. In this case, the total cross section of the subprocess depends of the contribution of the SM, which is to say, on the diagrams (1)-(3) and on the diagram (4) with anomalous couplings, such that,  $\sigma_{Tot} = \sigma_{SM} + \sigma_{Int}(\hat{a}_V, \hat{a}_A) + \sigma_{Anom}(\hat{a}_V^2, \hat{a}_A^2, \hat{a}_V\hat{a}_A)$ .

For the study of the process  $e^+e^- \rightarrow e^+\gamma^*e^- \rightarrow \bar{t}b\nu_e e^+$  in Fig. 7, we show the total cross section as a function of the electromagnetic form factors of the top quark  $\hat{a}_V$  and  $\hat{a}_A$  for  $P_{e^-,e^+} = -80\%, 0\%$  [61], two different center-of-mass energies  $\sqrt{s} = 1.4, 3 \text{ TeV}$  [14] and the

TABLE III: Bounds on the  $\hat{a}_V$  magnetic moment and  $\hat{a}_A$  electric dipole moment for the process  $e^+e^- \rightarrow e^+\gamma^*e^- \rightarrow \bar{t}b\nu_e e^+$  ( $\gamma^*$  is the Weizsacker-Williams photon) for  $Q^2 = 2 \text{ GeV}^2$ ,  $P_{e^-,e^+} = -80\%, 0\%$ ,  $b$  – tagging efficiency = 0.8,  $\delta_{sys} = 0\%, 5\%$  at  $2\sigma$  and  $3\sigma$  C.L.

$2\sigma$ C.L.		$\delta_{sys} = 0\%$		$\delta_{sys} = 5\%$	
$\sqrt{s} \text{ (TeV)}$	$\mathcal{L} \text{ (fb}^{-1}\text{)}$	$\hat{a}_V$	$ \hat{a}_A $	$\hat{a}_V$	$ \hat{a}_A $
1.4	50	[-0.3474, 0.4397]	0.3908	[-0.3669, 0.4592]	0.4104
1.4	300	[-0.2078, 0.3001]	0.2497	[-0.2647, 0.3570]	0.3074
1.4	500	[-0.1784, 0.2707]	0.2197	[-0.2505, 0.3428]	0.2931
1.4	1000	[-0.1443, 0.2366]	0.1848	[-0.2383, 0.3306]	0.2807
1.4	1500	[-0.1271, 0.2194]	0.1670	[-0.2339, 0.3262]	0.2762
3	50	[-0.1806, 0.2180]	0.1984	[-0.2037, 0.2411]	0.2216
3	300	[-0.1094, 0.1469]	0.1267	[-0.1652, 0.2026]	0.1829
3	500	[-0.0944, 0.1318]	0.1115	[-0.1608, 0.1982]	0.1785
3	1000	[-0.0769, 0.1144]	0.0937	[-0.1573, 0.1947]	0.1750
3	1500	[-0.0681, 0.1055]	0.0847	[-0.1561, 0.1935]	0.1738
3	2000	[-0.0547, 0.0921]	0.0713	[-0.1555, 0.1929]	0.1732
$3\sigma$ C.L.		$\delta_{sys} = 0\%$		$\delta_{sys} = 5\%$	
1.4	50	[-0.3827, 0.4750]	0.4264	[-0.4040, 0.4963]	0.4478
1.4	300	[-0.2302, 0.3225]	0.2724	[-0.2924, 0.3847]	0.3354
1.4	500	[-0.1980, 0.2903]	0.2397	[-0.2769, 0.3692]	0.3197
1.4	1000	[-0.1607, 0.2530]	0.2016	[-0.2636, 0.3559]	0.3063
1.4	1500	[-0.1418, 0.2341]	0.1822	[-0.2587, 0.3510]	0.3013
3	50	[-0.1986, 0.2360]	0.2165	[-0.2238, 0.2612]	0.2418
3	300	[-0.1208, 0.1583]	0.1383	[-0.1817, 0.2191]	0.1995
3	500	[-0.1044, 0.1419]	0.1217	[-0.1770, 0.2144]	0.1948
3	1000	[-0.0853, 0.1228]	0.1023	[-0.1732, 0.2106]	0.1909
3	1500	[-0.0756, 0.1131]	0.0924	[-0.1718, 0.2092]	0.1896
3	2000	[-0.0609, 0.1081]	0.0777	[-0.1711, 0.2086]	0.1890

Weizsacker-Williams photon virtuality  $Q^2 = 2 \text{ GeV}^2$  [65–68], respectively. We can see from this figure that the total cross section changes strongly with the variation of the  $\sqrt{s}$  values and this variation is of the order 20% at the ends of the range considered to  $\hat{a}_V$  and  $\hat{a}_A$ , which is to say,  $\hat{a}_{V,A} = \pm 1$ .

In Fig. 8 we summarize the respective limit contours for the dipole moments in the  $(\hat{a}_V - \hat{a}_A)$  plane for the process  $e^+e^- \rightarrow e^+\gamma^*e^- \rightarrow \bar{t}b\nu_e e^+$ . The curves are for  $\sqrt{s} = 1.4 \text{ TeV}$ ,  $\mathcal{L} = 50, 500, 1500 \text{ fb}^{-1}$  and  $\sqrt{s} = 3 \text{ TeV}$ ,  $\mathcal{L} = 50, 500, 2000 \text{ fb}^{-1}$ , respectively. We have used  $Q^2 = 2 \text{ GeV}^2$  and  $b$  – tagging efficiency = 0.8.

We determined the values numerical of the bounds obtained on the  $\hat{a}_V$  magnetic moment and  $\hat{a}_A$  electric dipole moment for  $b$  – tagging efficiency = 0.8, systematic uncertainties of  $\delta_{sys} = 0\%, 5\%$ ,  $\sqrt{s} = 1.4, 3 \text{ TeV}$ ,  $Q^2 = 2 \text{ GeV}^2$ , and  $\mathcal{L} = 50, 300, 500, 1000, 1500, 2000 \text{ fb}^{-1}$  at  $2\sigma$  and  $3\sigma$  in Table III. In this case, the bounds obtained for the dipole moments through the process  $e^+e^- \rightarrow e^+\gamma^*e^- \rightarrow \bar{t}b\nu_e e^+$  with polarized beams are slightly moderate with respect to those obtained by the process  $\gamma^*e^- \rightarrow \bar{t}b\nu_e$ , as is shown in Tables I and III, respectively. However, even in this case our results are competitive with the bounds reported in the literature [51–54].

## B. Top quark dipole moments through the process $e^+e^- \rightarrow e^+\gamma^*e^- \rightarrow \bar{t}b\nu_e e^+$ with unpolarized beams

As in the previous subsections, in this study, we search for  $e^+e^- \rightarrow e^+\gamma^*e^- \rightarrow \bar{t}b\nu_e e^+$  process to investigate  $t\bar{t}\gamma$  anomalous couplings, for this we present the cross section as a function of the anomalous couplings  $\hat{a}_V$  and  $\hat{a}_A$  for  $e^+e^- \rightarrow e^+\gamma^*e^- \rightarrow \bar{t}b\nu_e e^+$  in Fig. 9 for two different center-of-mass energies  $\sqrt{s} = 1.4, 3 \text{ TeV}$  and  $Q^2 = 2 \text{ GeV}^2$  [65–68]. From this figure is clear that the cross section is sensitive to the value of the center-of-mass energies and this sensitivity to  $\bar{t}b\nu_e e^+$  increases with the collider energy reaching a maximum at the end of the range considered, which is to say,  $\hat{a}_{V,A} = \pm 1$ . This variation of the cross section for  $\sqrt{s} = 1.4$  and  $3 \text{ TeV}$  is of the order 23%.

The resolving power of CLIC in the 2-dimensional space of  $\hat{a}_V$  and  $\hat{a}_A$  is shown in Fig. 10 for  $e^+e^- \rightarrow e^+\gamma^*e^- \rightarrow \bar{t}b\nu_e e^+$ , where  $\hat{a}_V$  and  $\hat{a}_A$  are the anomalous magnetic and electric and electric dipole moments of the  $t$ -quark. We consider the center-of-mass energies  $\sqrt{s} = 1.4, 3 \text{ TeV}$  and the luminosities of  $\mathcal{L} = 50, 500, 1500, 2000 \text{ fb}^{-1}$  planned

TABLE IV: Bounds on the  $\hat{a}_V$  magnetic moment and  $\hat{a}_A$  electric dipole moment for the process  $e^+e^- \rightarrow e^+\gamma^*e^- \rightarrow \bar{t}b\nu_e e^+$  ( $\gamma^*$  is the Weizsacker-Williams photon) for  $Q^2 = 2 \text{ GeV}^2$ ,  $b$  – tagging efficiency = 0.8,  $\delta_{sys} = 0\%$ , 5% at  $2\sigma$  and  $3\sigma$  C.L.

2 $\sigma$ C.L.		$\delta_{sys} = 0\%$		$\delta_{sys} = 5\%$	
$\sqrt{s} \text{ (TeV)}$	$\mathcal{L} \text{ (fb}^{-1}\text{)}$	$\hat{a}_V$	$ \hat{a}_A $	$\hat{a}_V$	$ \hat{a}_A $
1.4	50	[-0.4088, 0.5012]	0.4527	[-0.4219, 0.5142]	0.4657
1.4	300	[-0.2467, 0.3390]	0.2892	[-0.2883, 0.3806]	0.3313
1.4	500	[-0.2126, 0.0304]	0.2545	[-0.2673, 0.3597]	0.3101
1.4	1000	[-0.1728, 0.2651]	0.2140	[-0.2482, 0.3405]	0.2907
1.4	1500	[-0.1527, 0.2450]	0.1934	[-0.2409, 0.3332]	0.2833
3	50	[-0.2126, 0.2493]	0.2299	[-0.2274, 0.2654]	0.2459
3	300	[-0.1300, 0.1666]	0.1468	[-0.1726, 0.2106]	0.1908
3	500	[-0.1125, 0.1491]	0.1293	[-0.1656, 0.2035]	0.1838
3	1000	[-0.0921, 0.1287]	0.1086	[-0.1597, 0.1977]	0.1778
3	1500	[-0.0818, 0.1184]	0.0982	[-0.1576, 0.1956]	0.1757
3	2000	[-0.0662, 0.1028]	0.0826	[-0.1565, 0.1945]	0.1747
3 $\sigma$ C.L.		$\delta_{sys} = 0\%$		$\delta_{sys} = 5\%$	
1.4	50	[-0.4499, 0.5422]	0.4938	[-0.4641, 0.5554]	0.5081
1.4	300	[-0.2727, 0.3651]	0.3155	[-0.3182, 0.4105]	0.3614
1.4	500	[-0.2354, 0.3277]	0.2777	[-0.2953, 0.3876]	0.3383
1.4	1000	[-0.1919, 0.2842]	0.2335	[-0.2744, 0.3667]	0.3171
1.4	1500	[-0.1698, 0.2622]	0.2111	[-0.2664, 0.3587]	0.3091
3	50	[-0.2335, 0.2702]	0.2508	[-0.2497, 0.2877]	0.2682
3	300	[-0.1433, 0.1799]	0.1602	[-0.1899, 0.2279]	0.2082
3	500	[-0.1242, 0.1607]	0.1410	[-0.1822, 0.2202]	0.2005
3	1000	[-0.1019, 0.1385]	0.1185	[-0.1758, 0.2138]	0.1940
3	1500	[-0.0906, 0.1272]	0.1071	[-0.1735, 0.2115]	0.1917
3	2000	[-0.0736, 0.1102]	0.0901	[-0.1723, 0.2103]	0.1906

for the CLIC accelerator, with Weizsacker-Williams photon virtuality  $Q^2 = 2 \text{ GeV}^2$  and  $b$  – tagging efficiency = 0.8.

Finally, Table IV summarizes our results on the limits to the dipole moments of the top quark and for different values of the center-of-mass energy  $\sqrt{s} = 1.4, 3 \text{ TeV}$  and luminosity  $\mathcal{L} = 50, 300, 500, 1000, 1500, 2000 \text{ fb}^{-1}$ , we consider Weizsacker-Williams photon virtuality  $Q^2 = 2 \text{ GeV}^2$ ,  $b$  – tagging efficiency = 0.8 and considering the systematic uncertainties, which is to say,  $\delta_{sys} = 0\%, 5\%$ . These tables also list the measurement on the dipole moments  $\hat{a}_V$  and  $\hat{a}_A$  obtained at  $2\sigma$  and  $3\sigma$  C.L., respectively. The limits obtained on the dipole moments through the  $e^+e^- \rightarrow e^+\gamma^*e^- \rightarrow \bar{t}b\nu_e e^+$  single top quark production are competitive with the current limits reported in the literature [51–54].

#### IV. CONCLUSIONS

Even though  $\gamma e^-$  and  $\gamma\gamma$  processes require new equipment,  $\gamma^*e^-$  and  $\gamma^*\gamma^*$  are realized spontaneously at linear colliders without any equipment. These processes will allow the future linear colliders to operate in two different modes,  $\gamma^*e^-$  and  $\gamma^*\gamma^*$ , opening up the opportunity for a wider search for new physics. Therefore, the  $\gamma^*e^-$  linear collisions represent an excellent opportunity to study the sensibility on the anomalous magnetic moment and electric dipole moment of the top quark.

We have done a study of the total cross section of the processes  $\gamma e^- \rightarrow \bar{t}b\nu_e$  and  $e^+e^- \rightarrow e^+\gamma^*e^- \rightarrow \bar{t}b\nu_e e^+$ , with polarized and unpolarized and electron beams as a function of the anomalous couplings  $\hat{a}_V$  and  $\hat{a}_A$ . In addition, we investigate anomalous  $\hat{a}_V$  and  $\hat{a}_A$  couplings for both polarized and unpolarized cases. It does not change the general behavior of the cross sections of  $\hat{a}_V$  and  $\hat{a}_A$  couplings. However, we can see from figures that the polarization increases the cross sections according to the unpolarized case. The main reason of these results can be understood from Fig. 2. There are four diagrams which contribute to the process and one of them includes  $t\bar{t}\gamma$  vertex. This diagram gives the maximum contribution to the total cross section. For  $P_{e^-,e^+} = -80\%, 0\%$  case, this contribution is dominant due to the structure of the  $W e^- \nu_e$  vertex. Therefore, we can notice from these figures that polarization of the leptons can improve us the bounds on the anomalous couplings. The analysis is shown in Figs. 3, 5, and 7, 9 with Compton backscattering photon and Weizsacker-Williams photon virtuality of  $Q^2 = 2 \text{ GeV}^2$ ,  $b$  – tagging efficiency = 0.8, respectively. In



both processes, the cross section shows a strong dependence on the anomalous couplings  $\hat{a}_V$  and  $\hat{a}_A$ , as well as with the center-of-mass energy  $\sqrt{s}$ . This variation of the cross section for  $\sqrt{s} = 1.4, 3 \text{ TeV}$  is of the order 24.5%, 26.6% and 20%, 23% for  $\gamma e^- \rightarrow \bar{t} b \nu_e$  and  $e^+ e^- \rightarrow e^+ \gamma^* e^- \rightarrow \bar{t} b \nu_e e^+$ , respectively.

We also include contours plots for the dipole moments at the 95% *C.L.* in the  $(\hat{a}_V - \hat{a}_A)$  plane for the processes  $\gamma e^- \rightarrow \bar{t} b \nu_e$  and  $e^+ e^- \rightarrow e^+ \gamma^* e^- \rightarrow \bar{t} b \nu_e e^+$  for  $Q^2 = 2 \text{ GeV}^2$  and  $\sqrt{s} = 1.4, 3 \text{ TeV}$  in Figs. 4, 6 and 8, 10. The contours are consistent with the results obtained in Tables I-IV. From these tables we observe a strong correlation between the center-of-mass energy  $\sqrt{s}$ , integrated luminosity  $\mathcal{L}$  and the dipole moments  $\hat{a}_V$  and  $\hat{a}_A$ .

It is worth mentioning that our bounds obtained in Tables I-IV on the anomalous magnetic moment for the processes  $\gamma e^- \rightarrow \bar{t} b \nu_e$  and  $e^+ e^- \rightarrow e^+ \gamma^* e^- \rightarrow \bar{t} b \nu_e e^+$  for  $Q^2 = 2 \text{ GeV}^2$ ,  $\sqrt{s} = 1.4, 3 \text{ TeV}$ ,  $\mathcal{L} = 50, 300, 500, 1000, 1500, 2000 \text{ fb}^{-1}$ ,  $b$  – tagging efficiency = 0.8 and systematic errors of  $\delta_{sys} = 0\%, 5\%$  at  $2\sigma$  and  $3\sigma$  C.L. are competitive with those recently reported in the literature [51–54].

Others promising production modes for studying the cross section and the electromagnetic dipole moments  $\hat{a}_V$  and  $\hat{a}_A$  of the top quark is through the processes  $\gamma\gamma \rightarrow t\bar{t}$  (Compton backscattering photon),  $\gamma^*\gamma^* \rightarrow t\bar{t}$  (Weizsacker-Williams photon) and  $\gamma\gamma^* \rightarrow t\bar{t}$  (Compton backscattering photon, Weizsacker-Williams photon), respectively [97]. These processes are one of the most important sources of  $t\bar{t}$  pair production and represent new physics effects at a high-energy and high-luminosity linear electron positron collider such as the CLIC.

In conclusion, we have found that the processes  $\gamma e^- \rightarrow \bar{t} b \nu_e$  and  $e^+ e^- \rightarrow e^+ \gamma^* e^- \rightarrow \bar{t} b \nu_e e^+$  in the  $\gamma e^-$  and  $\gamma^* e^-$  collision modes at the high energies and luminosities expected at the CLIC can be used to probe for bounds on the magnetic moment  $\hat{a}_V$  and electric dipole moment  $\hat{a}_A$  of the top quark. In particular, we can appreciate that fixing the values for integrated luminosity of  $2 \text{ ab}^{-1}$ , center-of-mass energies of  $3 \text{ TeV}$ ,  $b$  – tagging efficiency = 0.8 and considering the systematic uncertainty, which is to say,  $\delta_{sys} = 5\%$  we derive bounds on the dipole moments of the top quark at  $2\sigma$  and  $3\sigma$  (90% and 95%) C.L.:  $-0.1112 (-0.1217) \leq \hat{a}_V \leq 0.1203 (0.1308)$ ,  $|\hat{a}_A| = 0.1156 (0.1261)$  and  $-0.1113 (-0.1218) \leq \hat{a}_V \leq 0.1204 (0.1309)$ ,  $|\hat{a}_A| = 0.1158 (0.1263)$  for  $\gamma e^- \rightarrow \bar{t} b \nu_e$  with unpolarized and polarized  $e^-$  beams and of  $-0.1555 (-0.1711) \leq \hat{a}_V \leq 0.1929 (0.2086)$ ,  $|\hat{a}_A| = 0.1732 (0.1890)$  and  $-0.1565 (-0.1723) \leq \hat{a}_V \leq 0.1945 (0.2103)$ ,  $|\hat{a}_A| = 0.1747 (0.1906)$  for  $e^+ e^- \rightarrow e^+ \gamma^* e^- \rightarrow \bar{t} b \nu_e e^+$  with unpolarized and polarized electron beams, which are compet-

itive with those recently reported in previous studies [51–54]. In addition, to our knowledge, our numerical results for the dipole moments of the top quark through the single top production processes have never been reported in the literature before and could be of relevance for the scientific community, since the studied processes are complementary to other top production mechanisms studied in the literature.

### Acknowledgments

A. G. R. acknowledges support from CONACyT, SNI and PROFOCIE (México).

- 
- [1] S. L. Glashow, *Nucl. Phys.* **22**, 579 (1961).
  - [2] S. Weinberg, *Phys. Rev. Lett.* **19**, 1264 (1967).
  - [3] A. Salam, in *Elementary Particle Theory*, Ed. N. Svartholm (Almquist and Wiskell, Stockholm, 1968) 367.
  - [4] K. A. Olive, *et al.*, [Particle Data Group], *Chin. Phys.* **C38**, 090001 (2014).
  - [5] ATLAS Collaboration, *Measurement of the inclusive  $t\bar{t}\gamma$  cross section with the ATLAS detector*, Tech. Rep. ATLAS-CONF-2011-153, ATLAS-COM-CONF-2011-186, 2011.
  - [6] CMS Collaboration, *Measurement of the inclusive top-quark pair + photon production cross section in the muon + jets channel in pp collisions at 8 TeV*, Tech. Rep. CMS-PAS-TOP-13-011, 2014.
  - [7] T. Abe, *et al.* [Am. LC Group], arXiv:hep-ex/0106055, arXiv:hep-ex/0106056, arXiv:hep-ex/0106057, arXiv:hep-ex/0106058, and references therein.
  - [8] G. Aarons, *et al.*, [ILC Collaboration], arXiv:0709.1893 [hep-ph].
  - [9] J. Brau, *et al.*, [ILC Collaboration], arXiv:0712.1950 [physics.acc-ph].
  - [10] H. Baer, T. Barklow, K. Fujii, *et al.*, arXiv:1306.6352 [hep-ph].

- [11] E. Accomando, *et al.*, [CLIC Phys. Working Group Collaboration], arXiv:hep-ph/0412251, CERN-2004-005.
- [12] D. Dannheim, P. Lebrun, L. Linssen, *et al.*, arXiv:1208.1402 [hep-ex].
- [13] J. A. Aguilar-Saavedra, *et al.*, [TESLA: The Superconducting electron positron linear collider with an integrated x-ray laser laboratory. Technical design report. Part 3. Physics at an  $e^+e^-$  linear collider], arXiv:hep-ph/0106315, and references therein.
- [14] H. Abramowicz, *et al.*, [The CLIC Detector and Physics Study], arXiv:1307.5288 [hep-ex].
- [15] A. Soni and R. M. Xu, *Phys. Rev. Lett.* **69**, 33 (1992).
- [16] A. Soni and R. M. Xu, *Phys. Rev.* **D45**, 2405 (1992).
- [17] A. Bartl, E. Christova, T. Gajdosik and W. Majerotto, *Nucl. Phys. Proc. Suppl.* **66**, 75 (1998).
- [18] W. Hollik, J. I. Illana, S. Rigolin, C. Schappacher and D. Stockinger, *Nucl. Phys.* **551B**, 3 (1999) [Erratum-ibid. **B557**, 407 (1999)].
- [19] C. S. Huang and T. J. Li, *Z. Phys.* **68C**, 319 (1995).
- [20] G. A. González-Sprinberg, R. Martínez and J. Vidal, *JHEP* **1107**, 094 (2011).
- [21] R. Martínez and J. Alexis Rodríguez, *Phys. Rev.* **D60**, 077504 (1999).
- [22] F. Larios, M. A. Pérez and C. P. Yuan, *Phys. Lett.* **B457**, 334 (1999).
- [23] D. Atwood, A. Aeppli and A. Soni, *Phys. Rev. Lett.* **69**, 2754 (1992).
- [24] P. Poulose and S. D. Rindani, *Phys. Rev.* **D57**, 5444 (1998) [Erratum-ibid. **D61**, 119902 (2000)].
- [25] S. Y. Choi and K. Hagiwara, *Phys. Lett.* **B359**, 369 (1995).
- [26] P. Poulose and S. D. Rindani, *Phys. Rev.* **D91**, 093008 (2015).
- [27] E. Boos, M. Dubinin, A. Pukhov, M. Sachwitz and H. J. Schreiber, *Eur. Phys. J.* **C21**, 81 (2001) and references therein.
- [28] Puneet Batra and Timothy M. P. Tait, *Phys. Rev.* **D74**, 054021 (2006).
- [29] J. Fuster, *et al.*, *Eur. Phys. J.* **C75**, 223 (2015) and references therein.
- [30] E. Boos and L. Dudko, *Int. J. Mod. Phys.* **A27**, 1230026 (2012) and references therein.
- [31] E. Boos, *Nucl. Instrum. Meth.* **A472**, 22 (2001) and references therein.
- [32] E. Boos, A. Pukhov, M. Sachwitz, H. J. Schreiber, *Phys. Lett.* **B404**, 119 (1997).
- [33] G. Jikia, *Nucl. Phys.* **B374**, 83 (1992).
- [34] E. Boos, *et al.*, *Z. Phys.* **C70**, 255 (1996).
- [35] E. Boos, *et al.*, *Z. Phys.* **C75**, 237 (1997).

- [36] Jun-Jie Cao, *et al.*, *Phys. Rev.* **D58**, 094004 (1998).
- [37] G. Weiglein, *et al.* [LHC/LC Study Group Collaboration], *Phys. Rept.* **426**, 47 (2006).
- [38] A. P. Heinson, A.S. Belyaev and E. E. Boos, *Phys. Rev.* **D56**, 3114 (1997).
- [39] D. O. Carlson and C.P. Yuan, *Phys. Lett.* **B306**, 386 (1993).
- [40] D. O. Carlson, E. Malkawi and C. P. Yuan, *Phys. Lett.* **B337**, 145 (1994).
- [41] E. H. Simmons, *Phys. Rev.* **D55**, 5494 (1997).
- [42] D. Atwood, S. Bar-Shalom, G. Eilam and A. Soni, *Phys. Rev.* **D54**, 5412 (1996).
- [43] C. S. Li, R. J. Oakes and J. M. Yang, *Phys. Rev.* **D55**, 1672 (1997).
- [44] E. Malkawi and T. Tait, *Phys. Rev.* **D54**, 5758 (1996).
- [45] A. Datta, J. M. Yang, B. Young and X. Zhang, *Phys. Rev.* **D56**, 3107 (1997).
- [46] R. J. Oakes, K. Whisnant, J. M. Yang, B. Young and X. Zhang, *Phys. Rev.* **D57**, 534 (1998).
- [47] W. Bernreuther, *et al.*, *Phys. Rev. Lett.* **95**, 261802 (2005) and references therein.
- [48] M. E. Pospelov and I. B. Khriplovich, *Sov. J. Nucl. Phys.* **53**, 638 (1991) [*Yad. Fiz.* 53 (1991) 1030].
- [49] F. Hoogeveen, *Nucl. Phys.* **B341**, 322 (1990).
- [50] T. Ibrahim and P. Nath, *Phys. Rev.* **D82**, 055001 (2010).
- [51] U. Baur, A. Juste, L. H. Orr and D. Rainwater, *Phys. Rev.* **D71**, 054013 (2005).
- [52] A. O. Bouzas and F. Larios, *Phys. Rev.* **D87**, 074015 (2013).
- [53] A. O. Bouzas and F. Larios, *Phys. Rev.* **D88**, 094007 (2013).
- [54] Sh. Fayazbakhsh, S. Taheri Monfared and M. Mohammadi Najafabadi, *Phys. Rev.* **D92**, 014006 (2015).
- [55] M. S. Amjad, *et al.*, arXiv:1307.8102 [hep-ph], and references therein..
- [56] A. Juste, *et al.*, arXiv:hep-ph/0601112, and references therein.
- [57] D. Asner, *et al.*, arXiv:1307.8265 [hep-ex] and references therein.
- [58] J. F. Kamenik, M. Papucci and A. Weiler, *Phys. Rev.* **D85**, 071501 (2012).
- [59] J. A. Aguilar-Saavedra, *Nucl. Phys.* **B812**, 181 (2009).
- [60] J. A. Aguilar-Saavedra, M. C. N. Fiolhais and A. Onofre, *JHEP* **07**, 180 (2012).
- [61] G. Moortgat-Pick, *et al.*, *Physics Reports* **460**, 131243 (2008).
- [62] G. Baur, *et al.*, *Phys. Rep.* **364**, 359 (2002).
- [63] V. M. Budnev, I. F. Ginzburg, G. V. Meledin and V. G. Serbo, *Phys. Rep.* **15**, 181 (1975).
- [64] K. Piotrkowski, *Phys. Rev.* **D63**, 071502 (2001).

- [65] M. Acciarri, *et al.*, [L3 Collaboration], *Phys. Lett.* **B434**, 169 (1998).
- [66] K. Ackerstaff, *et al.*, [OPAL Collaboration], *Phys. Lett.* **B431**, 188 (1998).
- [67] I. Sahin, *Phys. Rev.* **D85**, 033002 (2012).
- [68] A. A. Billur, *et al.*, *Phys. Rev.* **D89**, 037301 (2014).
- [69] A. Abulencia, *et al.*, [CDF Collaboration], *Phys. Rev. Lett.* **98**, 112001 (2007).
- [70] T. Aaltonen, *et al.*, [CDF Collaboration], *Phys. Rev. Lett.* **102**, 222002 (2009).
- [71] T. Aaltonen, *et al.*, [CDF Collaboration], *Phys. Rev. Lett.* **102**, 242001 (2009).
- [72] S. Chatrchyan, *et al.*, [CMS Collaboration], *JHEP* **1201**, 052 (2012).
- [73] S. Chatrchyan, *et al.*, [CMS Collaboration], *JHEP* **1211**, 080 (2012).
- [74] V. M. Abazov, *et al.*, [D0 Collaboration], *Phys. Rev.* **D88**, 012005 (2013).
- [75] S. Chatrchyan, *et al.*, [CMS Collaboration], *JHEP* **07**, 116 (2013).
- [76] S. C. Inan, *Phys. Rev.* **D81**, 115002 (2010).
- [77] S. C. Inan, *Nucl. Phys.* **B897**, 289 (2015).
- [78] S. C. Inan, *Int. J. Mod. Phys.* **A26**, 3605 (2011).
- [79] I. Sahin and S. C. Inan, *JHEP* **0909**, 069 (2009).
- [80] S. Atag, S. C. Inan and I. Sahin, *JHEP* **1009**, 042 (2010).
- [81] I. Sahin and B. Sahin, *Phys. Rev.* **D86**, 115001 (2012).
- [82] B. Sahin and A. A. Billur, *Phys. Rev.* **D86**, 074026 (2012).
- [83] A. Senol, *Int. J. Mod. Phys.* **A29**, 1450148 (2014).
- [84] A. Senol, *Phys. Rev.* **D87**, 073003 (2013).
- [85] S. Fichet, G. von Gersdorff, B. Lenzi, C. Royon and M. Saimpert, *JHEP* **1502**, 165 (2015).
- [86] H. Sun, *Phys. Rev.* **D90**, 035018 (2014).
- [87] H. Sun, *Nucl. Phys.* **B886**, 691 (2014).
- [88] H. Sun, Y. J. Zhou and H. S. Hou, *JHEP* **1502**, 064 (2015).
- [89] A. Senol and M. Koksar, *JHEP* **1503**, 139 (2015).
- [90] S. Atag and A. A. Billur, *JHEP* **1011**, 060 (2010).
- [91] A. Belyaev, N. D. Christensen and A. Pukhov, *Comput. Phys. Commun.* **184**, 1729 (2013).
- [92] A. Pukhov, *et al.*, CalcHEP a package for evaluation of Feynman diagrams and integration over multiparticle phase space, Report No. INP MSU 98-41/542, arXiv:hep-ph/9908288; arXiv:hep-ph/0412191.
- [93] G. Aad, *et al.*, [ATLAS Collaboration], *Phys. Lett.* **B717**, 330 (2012).

- [94] G. Abbiendi, *et al.*, [OPAL Collaboration], *Phys. Lett.* **B521**, 181 (2001).
- [95] M. Martinez and R. Miquel, *Eur. Phys. J.* **C27**, 49 (2003).
- [96] A. Juste, M. Martinez and D. Schulte, *Linear Collider: Physics and Detector Studies Parte E*. Contributions to the Workshop, Frascati, London, Munich, Hamburg, February 1996 to November 1996. ed. R. Settles, DESY Report 97-123E.
- [97] A. A. Billur, A. Gutiérrez-Rodríguez and M. Köksal, Work in progress.

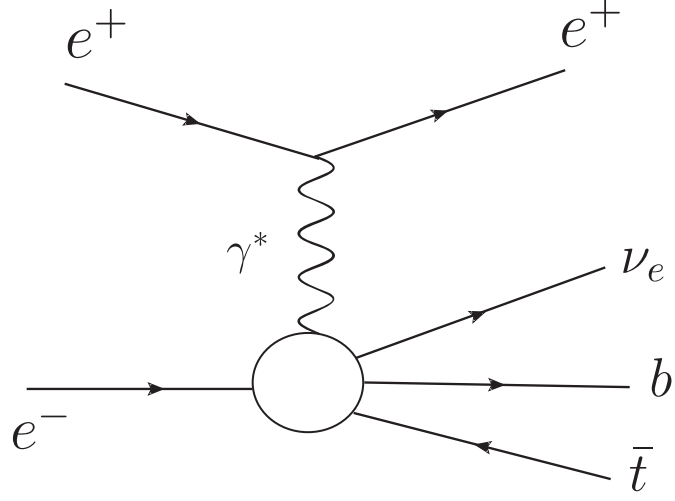


FIG. 1: Schematic diagram for the process of single top quark production  $e^+e^- \rightarrow e^+\gamma^*e^- \rightarrow \bar{t}b\nu_e e^+$ .

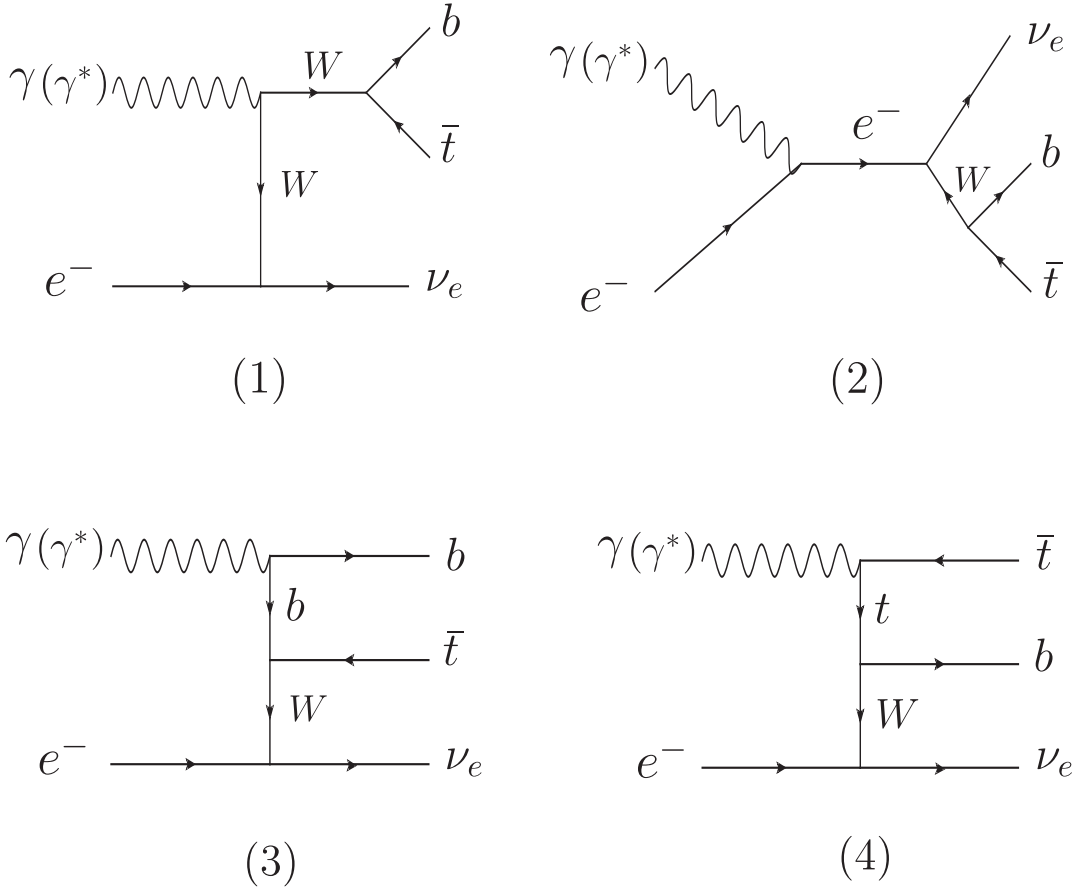


FIG. 2: The Feynman diagrams contributing to the process  $\gamma e^- \rightarrow \bar{t}b\nu_e$  and the subprocess  $\gamma^* e^- \rightarrow \bar{t}b\nu_e$ .

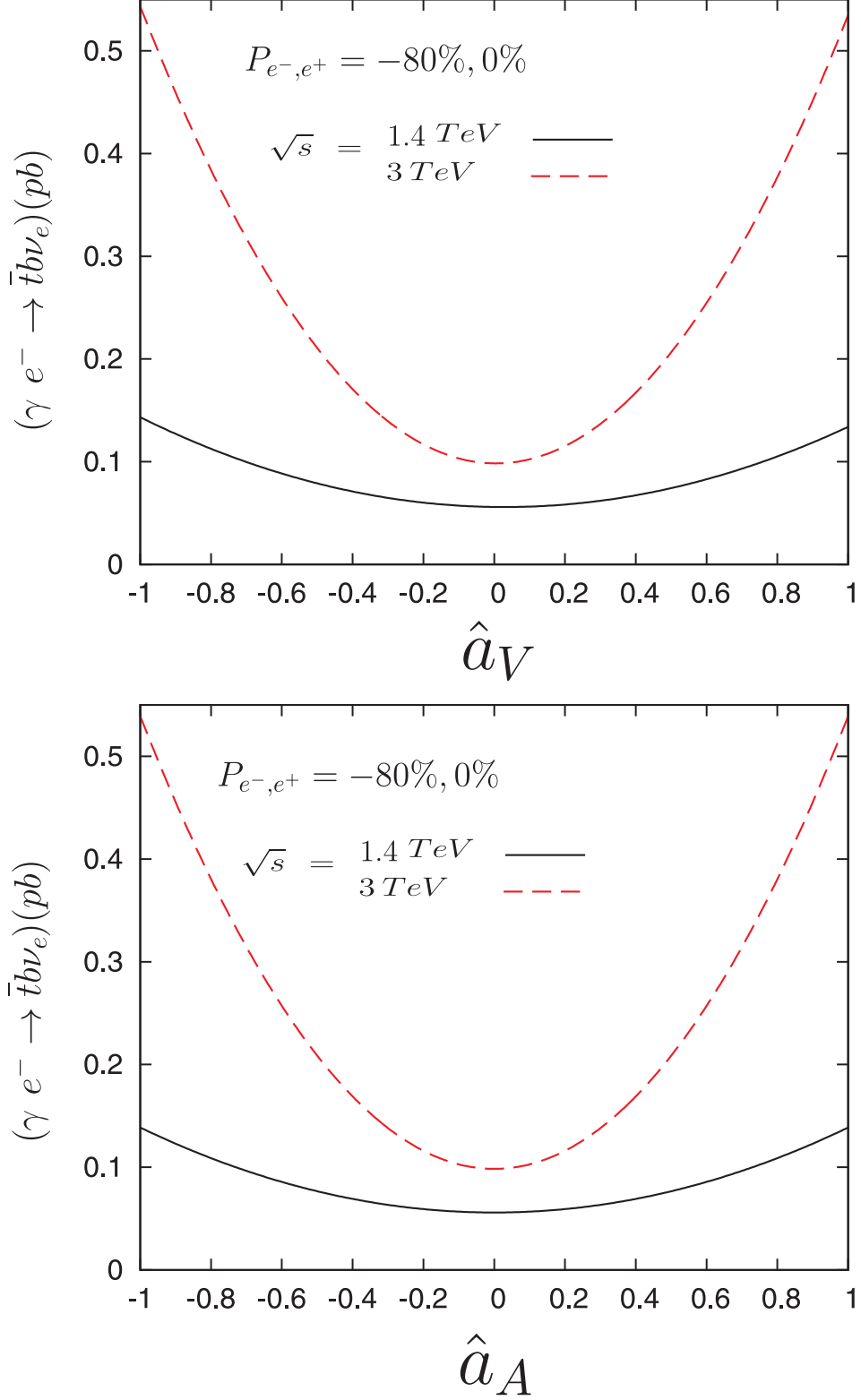


FIG. 3: The integrated total cross section of the process  $\gamma e^- \rightarrow \bar{t} b \nu_e$  ( $\gamma$  is the Compton backscattering photon) as a function of  $\hat{a}_V$  and  $\hat{a}_A$  with  $P_{e^-,e^+} = -80\%, 0\%$  and  $\sqrt{s} = 1.4, 3 \text{ TeV}$ , respectively.



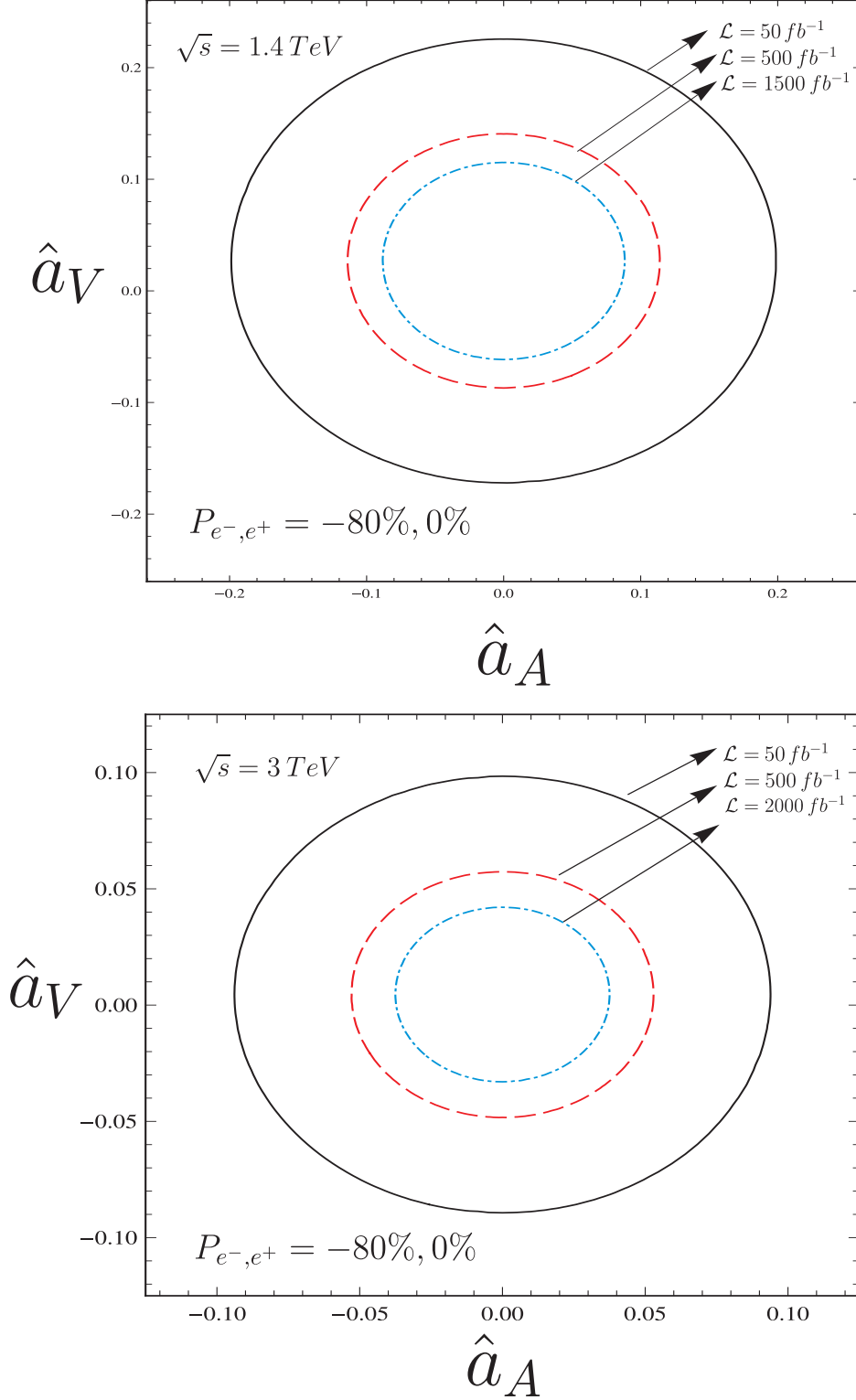


FIG. 4: Limits contours at the 95% *C.L.* in the  $\hat{a}_V$  -  $\hat{a}_A$  plane for  $\gamma e^- \rightarrow \bar{t} b \nu_e$  ( $\gamma$  is the Compton backscattering photon) with  $P_{e^-, e^+} = -80\%, 0\%$  and  $\sqrt{s} = 1.4, 3 \text{ TeV}$ , respectively.

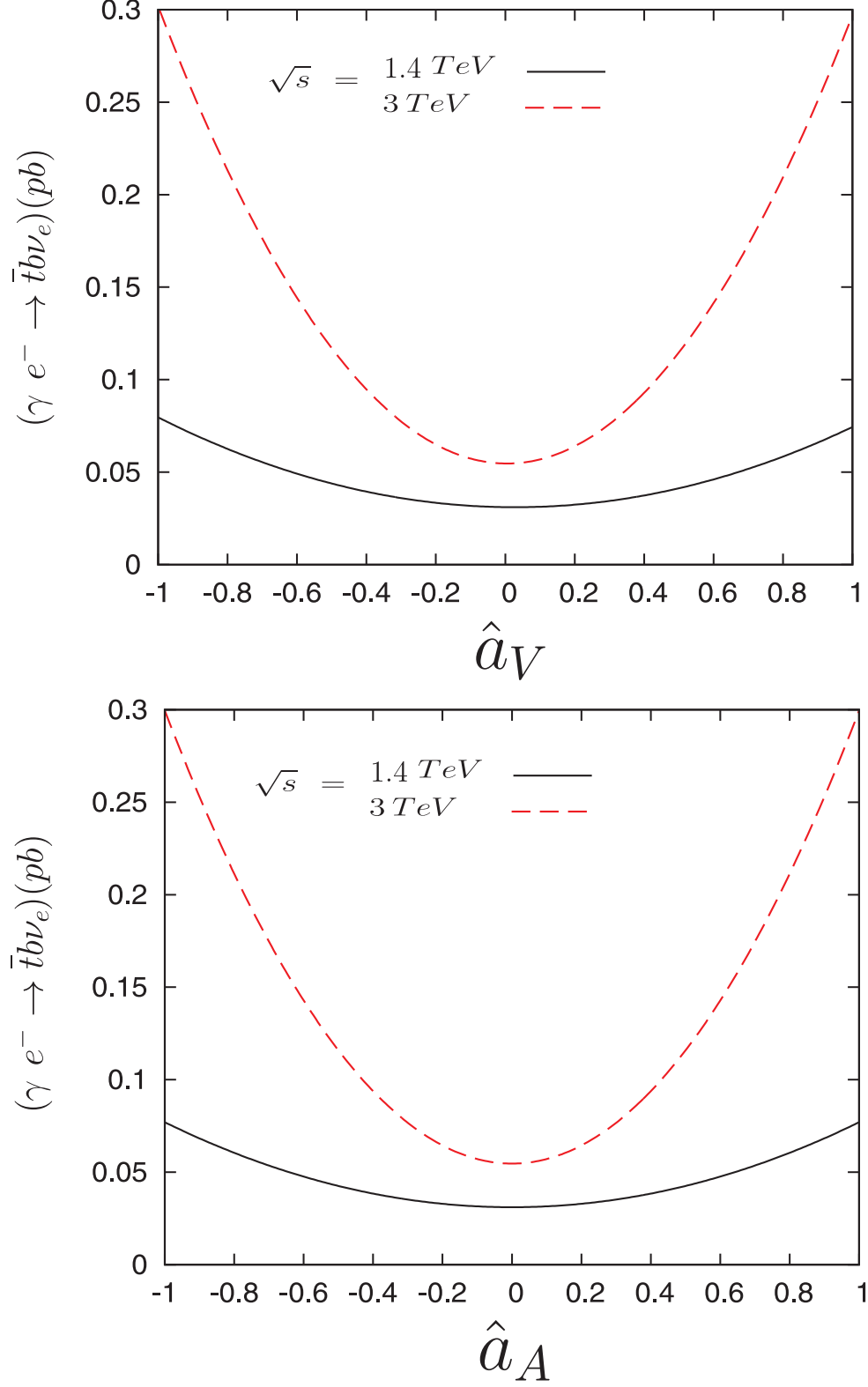


FIG. 5: The integrated total cross section of the process  $\gamma e^- \rightarrow \bar{t} b \nu_e$  ( $\gamma$  is the Compton backscattering photon) as a function of  $\hat{a}_V$  and  $\hat{a}_A$  with  $\sqrt{s} = 1.4, 3 \text{ TeV}$ .

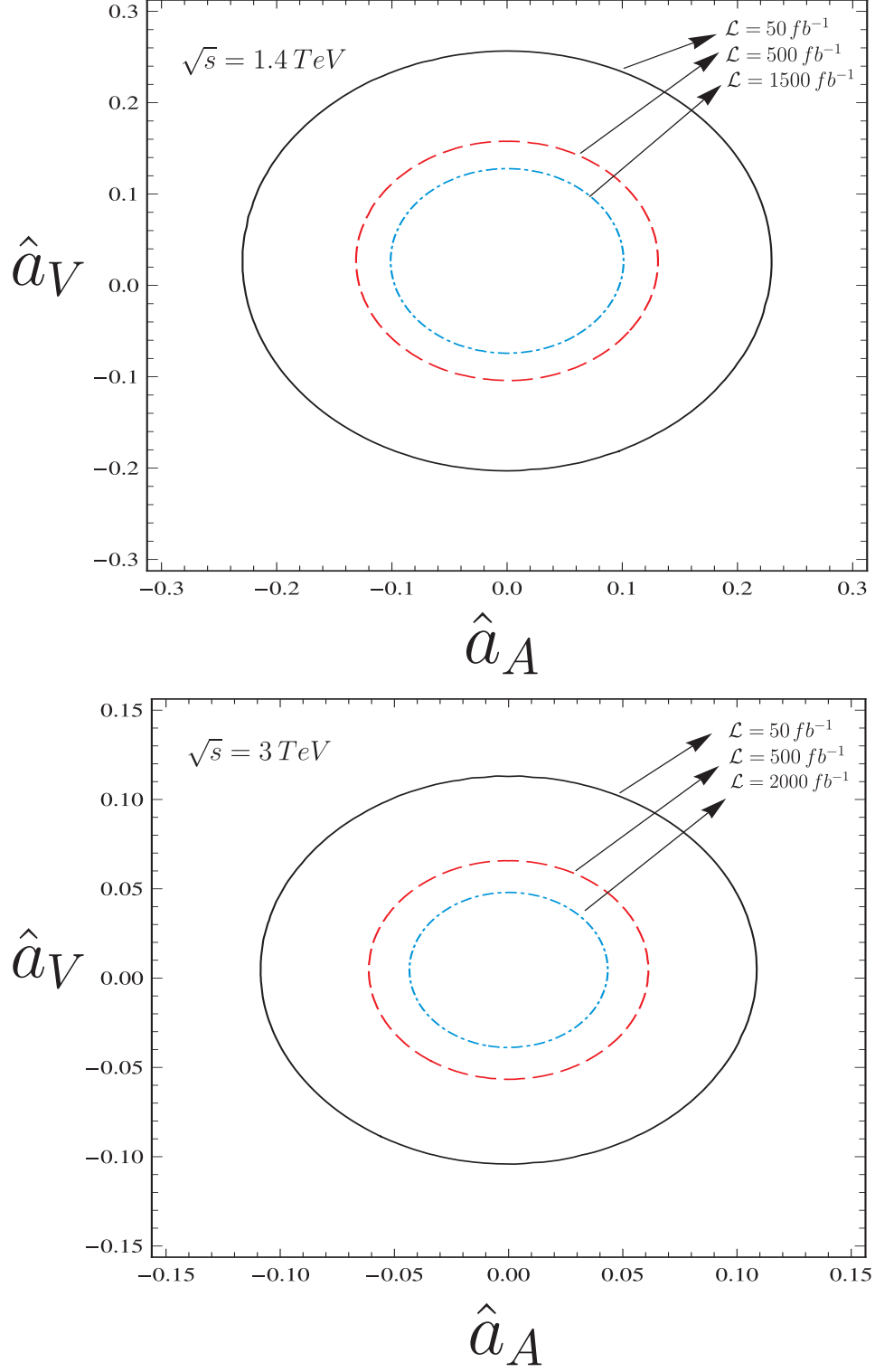


FIG. 6: Limits contours at the 95% *C.L.* in the  $\hat{a}_V$  -  $\hat{a}_A$  plane for  $\gamma e^- \rightarrow \bar{t} b \nu_e$  ( $\gamma$  is the Compton backscattering photon) with  $\sqrt{s} = 1.4, 3 \text{ TeV}$ .

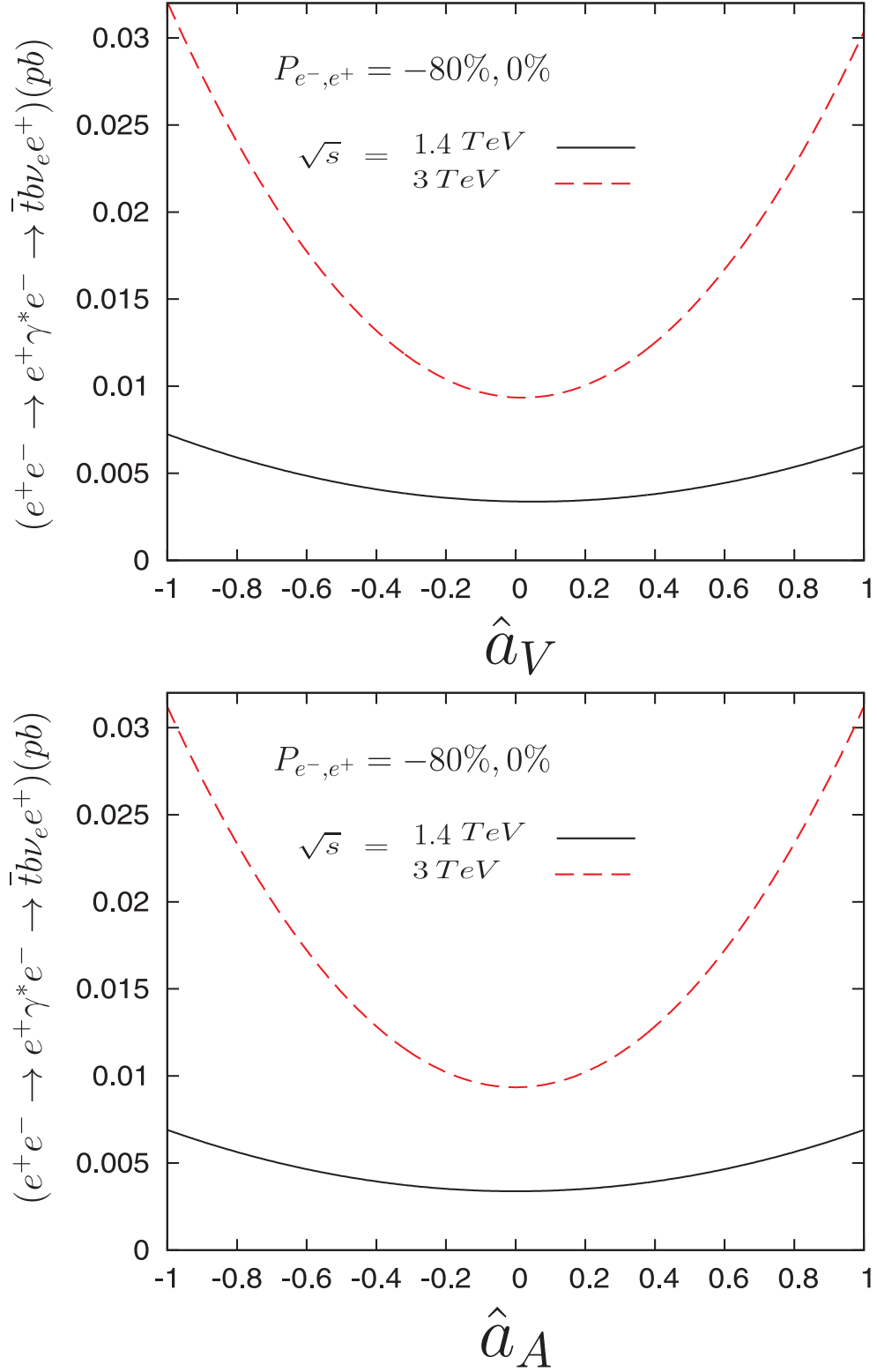


FIG. 7: The integrated total cross section of the process  $e^+e^- \rightarrow e^+\gamma^*e^- \rightarrow \bar{t}b\nu_e e^+$  ( $\gamma^*$  is the Weizsacker-Williams photon) as a function of  $\hat{a}_V$  and  $\hat{a}_A$  with  $P_{e^-,e^+} = -80\%, 0\%$ ,  $\sqrt{s} = 1.4, 3 TeV$  and  $Q^2 = 2 GeV^2$ .

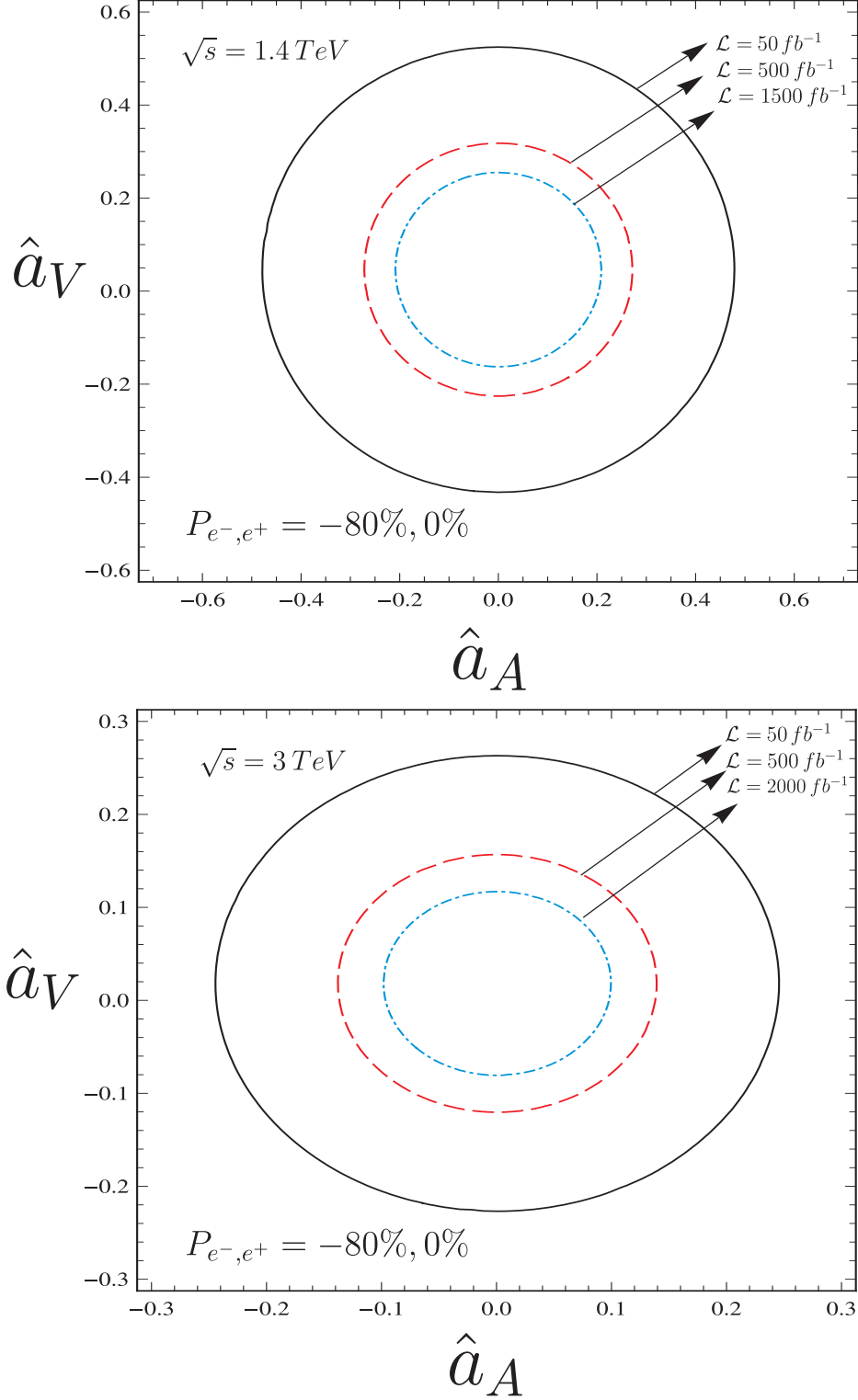


FIG. 8: Limits contours at the 95% *C.L.* in the  $\hat{a}_V$  -  $\hat{a}_A$  plane for  $e^+e^- \rightarrow e^+\gamma^*e^- \rightarrow t\bar{b}\nu_e e^+$  ( $\gamma^*$  is the Weizsacker-Williams photon) with  $P_{e^-,e^+} = -80\%, 0\%$ ,  $\sqrt{s} = 1.4, 3 \text{ TeV}$  and  $Q^2 = 2 \text{ GeV}^2$ .

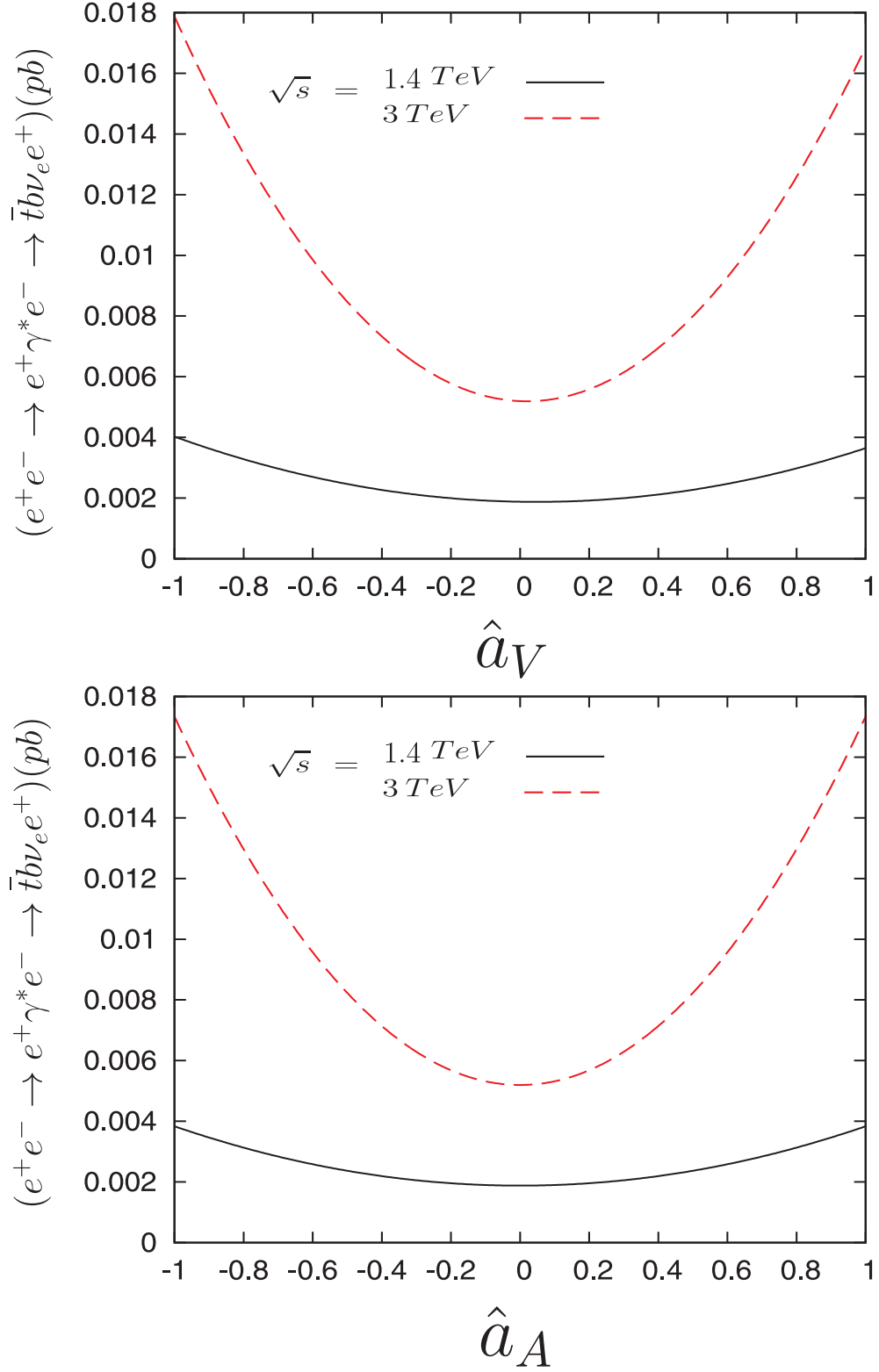


FIG. 9: The integrated total cross section of the process  $e^+e^- \rightarrow e^+\gamma^*e^- \rightarrow \bar{t}b\nu_e e^+$  ( $\gamma^*$  is the Weizsacker-Williams photon) as a function of  $\hat{a}_V$  and  $\hat{a}_A$  with  $\sqrt{s} = 1.4, 3 TeV$  and  $Q^2 = 2 GeV^2$ .

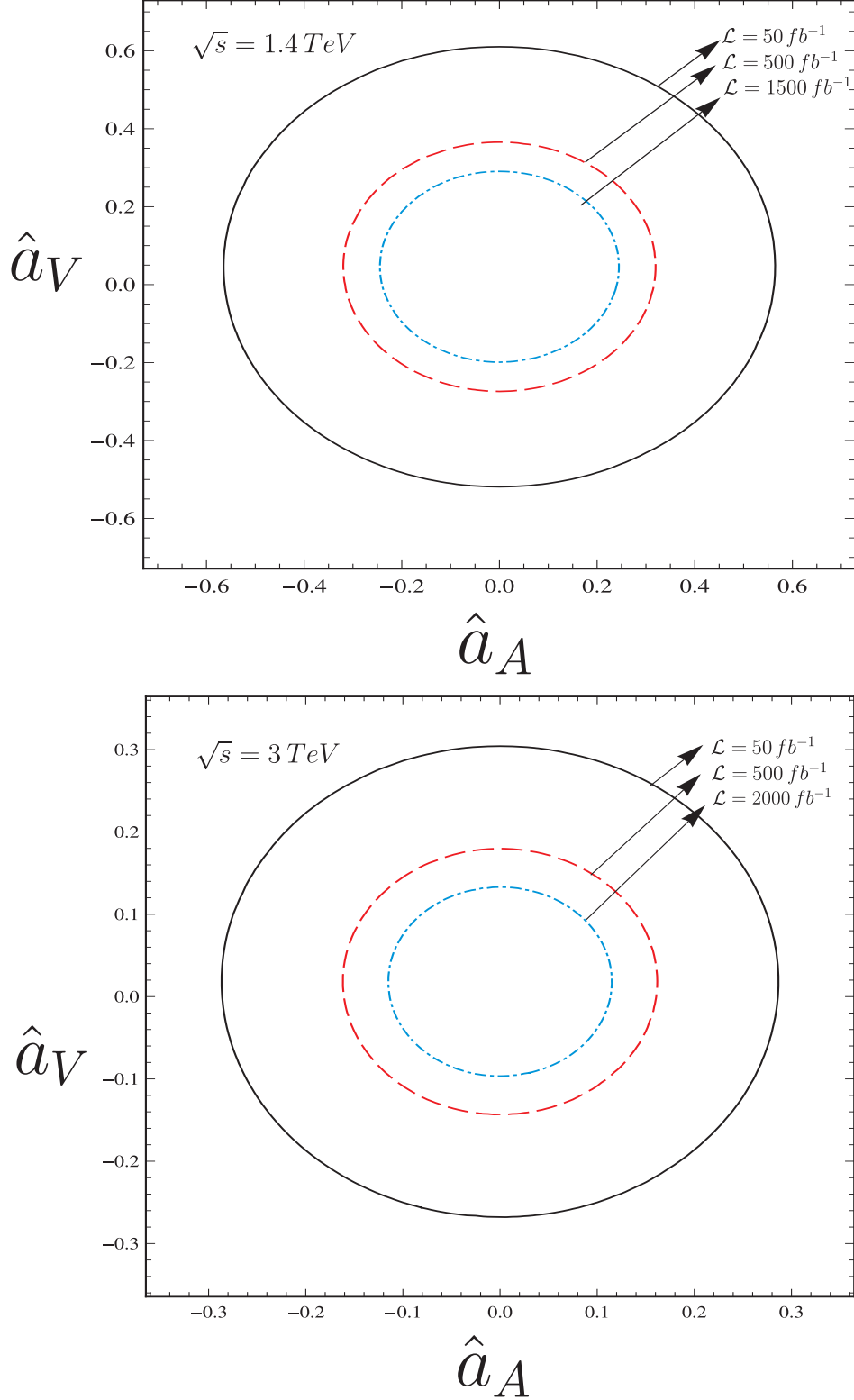


FIG. 10: Limits contours at the 95% *C.L.* in the  $\hat{a}_V$  -  $\hat{a}_A$  plane for  $e^+e^- \rightarrow e^+\gamma^*e^- \rightarrow \bar{t}b\nu_e e^+$  ( $\gamma^*$  is the Weizsacker-Williams photon) with  $\sqrt{s} = 1.4, 3 \text{ TeV}$  and  $Q^2 = 2 \text{ GeV}^2$ .